Combustion and Flame 254 (2023) 112785

Contents lists available at ScienceDirect

Combustion and Flame

journal homepage: www.elsevier.com/locate/combustflame

High pressure oxidation of NH_3/*n*-heptane mixtures

Lauge S. Thorsen[a], Malene S.T. Jensen[a], Mille S. Pullich[a], Jakob M. Christensen[a], Hamid Hashemi[a], Peter Glarborg[a], Vladimir A. Alekseev[b], Elna J.K. Nilsson[b,*], Ziyu Wang[c], Bowen Mei[c], Ning Liu[c], Yiguang Ju[c]

[a] Department of Chemical and Biochemical Engineering, Technical University of Denmark (DTU), Lyngby DK-2800, Denmark
[b] Division of Combustion Physics, Lund University, Sweden
[c] Department of Mechanical and Aerospace Engineering, Princeton University, NJ 08544, USA

ARTICLE INFO

Article history:
Received 17 October 2022
Revised 11 April 2023
Accepted 11 April 2023
Available online 17 May 2023

Keywords:
N-heptane/NH_3
Ignition delay time
Flow reactor
Perfectly stirred reactor
Detailed Kinetic Mechanism

ABSTRACT

Oxidation of NH_3/*n*-heptane mixtures at pressures up to 100 atm and temperatures of 400–900 K was characterized experimentally in a laminar flow reactor and a jet-stirred reactor. A detailed chemical kinetic model was developed, updating the hydrogen and amine subsets and introducing a subset for the chemical coupling with emphasis on the NH_2 + *n*-heptane reaction. The kinetic model provided a good prediction of the ignition delay times measured in a rapid compression machine by Yu et al. (Combust. Flame 217 (2020) 2–11) as well as the high pressure experimental data obtained in the present work. The results show that it is important to include updated rate constants for NH_2 + HO_2 and NH_2 + *n*-C_7H_{16} to obtain reliable predictions for ignition and oxidation of NH_3/*n*-heptane mixtures at high pressure. The effectiveness of implementing analogy rules for determining the rate constant of the key reaction NH_2 + *n*-C_7H_{16} was confirmed by the observed results.

1. Introduction

To reduce the impact of combustion on the climate change, there is an incentive for a transition from fossil energy to a low-carbon economy. Ammonia (NH_3) is a carbon-free fuel and can be a suitable alternative for stationary power, transportation, and energy storage applications. The feasibility of using ammonia in engines and gas turbines is being investigated extensively [1–3]. The use of NH_3 as an engine fuel is challenging due to its poor combustion characteristics such as a long ignition delay time and a low flame speed. This short-coming can be partly or fully overcome by use of a co-fuel mixture such as hydrogen or diesel fuel addition into ammonia [4].

In terms of compression-ignition engines, using diesel as a pilot- or co-fuel is considered as a promising approach. Co-combustion of diesel and ammonia has been tested in diesel engines [5–10]. Results indicate that this fuel mixture has a significant potential, allowing operation with up to 95% NH_3 energy input. However, there are challenges related to comparatively low combustion temperatures, unburned ammonia, and N_2O emissions, and advanced diesel injection strategies may be required to alleviate these problems [6].

Use of computational fluid dynamics (CFD) including finite rate chemistry, is an attractive option in the design and optimization of ammonia/diesel-fuelled engines. To be computationally feasible, these simulations require accurate but compact chemical kinetic mechanism. However, the knowledge of the detailed kinetics of ignition and oxidation of this fuel mixture is limited, which hampers the development of the reduced kinetic mechanisms. Experimentally determined ignition delay times for ammonia/diesel have been reported from Rapid Compression Machines (RCM) [11,12]. A blended mechanism was used to interpret the data [11], but analysis was made difficult by the complexity of the diesel fuel. In the following work [12], predictions of the main ignition were significantly improved due to introduction of ammonia-diesel cross interactions, however, some discrepancies remained in terms of the first ignition. Understanding of the interactions of N-species with a heavy hydrocarbon fuel can more easily be reached by studying blends of ammonia with a single-component hydrocarbon fuel. To facilitate modeling and interpretation of the behavior of ammonia/diesel mixtures, it is therefore of interest to study the ignition and oxidation of NH_3 mixed with *n*-heptane (C_7H_{16}); a common diesel surrogate.

* Corresponding author.
E-mail address: Elna.Heimdal_Nilsson@forbrf.lth.se (E.J.K. Nilsson).

https://doi.org/10.1016/j.combustflame.2023.112785

Several studies of the high-pressure chemistry of ammonia and *n*-heptane, respectively, are available in the literature. Results include ignition delay measurements for ammonia [13–16] and *n*-heptane [17–20], as well as flow reactor results for the oxidation of each of the two fuels [21,22]. Experimental results are scarce for ammonia/*n*-heptane mixtures, but data at elevated pressure have been reported for ignition delays in RCM (635–945 K, 10–15 bar) by Yu et al. [23]. In addition, results at lower pressure are available for flame speeds [24] and species profiles in jet-stirred reactors [25].

A number of models for *n*-heptane ignition have been reported [20,26–30] that generally predict the ignition behavior well. Thorsen et al. [31] concluded that the mechanism of Zhang et al. [20] is performing best for a range of experimental cases [32–34]. In addition to that, it also provides the best agreement in terms of oxidation of *n*-heptane in high-pressure flow reactors [22]. For ammonia, several mechanisms have been published in recent years. Models by Mathieu and Petersen [13], Li et al. [35], Otomo et al. [36], Glarborg et al. [37], Mei et al. [38,39], Stagni et al. [40], and Jiang et al. [41] were tested by Valera-Medina et al. [3] who concluded that none of them provided accurate predictions over wider range of conditions, covering various reactor configurations.

Available mechanisms for NH_3/*n*-heptane mixtures are based on merging subsets for *n*-heptane and ammonia, assuming little direct interaction. Yu et al. [23] combined the *n*-heptane mechanism of Zhang et al. [20] with the amine subset from Glarborg et al. [37]. Compared to experiment, their modeling showed substantially longer ignition times at lower temperatures and overestimated the NTC initiation temperature. The authors speculated that the two possible reasons for these differences might be the performance of the NH_3 submechanism at low temperatures and/or absence of cross reactions between nitrogen and carbon chemistryg [23], outlining the direction for future work. Lubrano Lavadera et al. [24] adopted the model developed at Polimi [40,42], which provided a good description of the measured flame speeds. They concluded that for flame propagation direct chemical coupling effects could be disregarded.

Due to the scarcity of both experimental data and modeling studies, the importance of the chemical coupling for high pressure ignition and oxidation of mixtures of NH_3 with *n*-heptane is still an open question. The C/H/N/O chemistry has been studied extensively for C_1–C_2 hydrocarbons [37], but few studies are available for larger hydrocarbons. Interactions include H-abstraction from hydrocarbons by radicals such as NH_2 and CN, as well as reactions involving NO and NO_2 with hydrocarbon and peroxide radicals. These steps may affect ignition as well as pollutant emissions.

Previous experiments for ignition and oxidation of NH_3/*n*-heptane fuel mixtures were conducted at pressures well below those of engines and gas turbines. In the present work, experiments are conducted at pressures up to 100 atm in the DTU laminar flow reactor and the Princeton supercritical pressure jet-stirred reactor to characterize the high-pressure features of this fuel mixture. The experiments are conducted at very high dilution to prevent overheating. Such mixtures do not fully represent conditions that occur in a real engine, however, as all elementary reactions retain the values of their rate constants, experimental investigations in these idealized conditions do provide valuable information for development of models for engine combustion. Moreover, in such systems (JSR or FR), chemical kinetics is decoupled from effects related to diffusion.

A detailed chemical kinetic model for the ignition and oxidation of NH_3/*n*-heptane is established. Similar to Yu et al. [23], we base the mechanism on merging the *n*-heptane mechanism of Zhang et al. [20] with the amine subset from Glarborg et al. [37]. However, we include a novel subset for the chemical coupling reactions, based on analogy with similar reactions for smaller fuels. Furthermore, the H_2-O_2 and amine subsets have been updated (Zhao et al. [43] and Glarborg [44], respectively) to include newly published elementary reactions involving HO_2 chemistry. The revised model is validated against the present experimental results, as well as the ignition delay times reported by Yu et al. [23], and the key reactions are identified.

2. Experimental

2.1. High-pressure flow reactor

The DTU high-pressure flow reactor is designed to operate at pressures up to 100 bar. A brief description is given here as the setup is described in detail elsewhere [22,45,46]. The reactor is a 154 cm long quartz tube with 8 mm ID (inner diameter) and 10 mm OD (outer diameter). A steel container surrounds the quartz tube and the cavity between the steel container and quartz tube is pressurized to form a pressure shell preventing high pressure gradients over the quartz tube. A moveable thermostat is placed inside the steel container to estimate the temperature inside the reactor. Heating tape ($\sim$ 373 K) is used downstream to prevent product condensation.

High pressure mass flow controllers are used to control the feed of the reactant gasses (ammonia, *n*-heptane and O_2) and nitrogen (for dilution). Gas bottles from Air Liquid with certified concentrations of $\pm$2% were used. The total mass flow was maintained around 1500 Nml/min, allowing a good plug-flow approximation in the laminar flow regime [45]. Temperature profiles in the reactor at inert conditions were measured as shown in Fig. S1 in Supplementary Material. We define the isothermal zone to be the length of the reactor where the temperature is within $\pm$6 K. The isothermal zone was measured to be 45–48 cm at 21 bar and 39–45 cm at 100 bar, corresponding to residence times of 6–10 s at 21 bar and 28–57 s at 100 bar, decreasing with temperature.

The downstream was analysed for products using a Trace 1300/1310 gas chromatograph (GC) from Thermo Fisher for hydrocarbons, O_2, CO and CO_2, and ammonia levels were measured using either an FTIR analyzer (MKS multigas 2030) or a dedicated NH_3 analyzer (ABB AO2020). The GC uses a Flame Ionization Detector (FID) with a capillary column Rtx-5, and a Thermal Conductivity Detector (TCD) with three micro packed columns; Rt-XLSulfur, Molsieve-5A, and HS-N (HayeSep). The GC was calibrated for *n*-heptane, butane, *iso*-butene, propane, propene, ethane, ethene, methane, methanol, acetaldehyde, CO, CO_2, and O_2. For every measuring temperature, two to five GC samples were collected to determine the species mole fractions with a measuring uncertainty within 10%. Additional uncertainty factors contributing to the overall systematic error of the experiments include wall reactions, mixing, temperature inhomogeneities, etc. They are more difficult to quantify, so that the overall experimental uncertainty can be expected to be higher, however, as will be shown in the following, the experimental trends are captured well by the present kinetic mechanism, in which, no rate constant was modified or tuned to fit the experimental data analyzed in this study.

2.2. Supercritical pressure jet-stirred reactor

The supercritical pressure jet-stirred reactor (SP-JSR) recently developed at Princeton was employed to conduct oxidation studies of NH_3/*n*-heptane mixtures at low and intermediate temperatures and at 100 atm. The core part of the SP-JSR was a quartz sphere with an internal volume of 0.4 cm^3. The center of the sphere had eight perpendicular nozzles with 0.2 mm inner diameter on four jet fingers. This geometry generates homogeneous mixing [47]. The reactor was placed inside a stainless-steel shell

with several segments of electric heating wires. The axial temperature profiles were within ± 5 K under the experimental conditions. The velocity distribution profiles of the sphere cross section and the temperature profile measurements are provided in an earlier publication [47]. The gas flow rates were controlled by several high-pressure mass flow controllers (Brooks, SLA5800). The liquid fuel (*n*-heptane, Sigma-Aldrich, ≥99.5%) was injected into a vaporization line by a high-pressure syringe pump (Harvard PHD). The products at the exit of the sphere were sampled through a quartz sonic nozzle into a vacuum environment created by a dry pump. The NH_3 mole fractions were measured by a multi-pass Herriot cell for tunable diode laser absorption spectroscopy (TDLAS) at 1726.4 cm^{-1} wavenumber. The other gas samples were quantified with a micro gas chromatography (μ-GC). The uncertainty of the measurements was less than 5%. For the overall uncertainty, same considerations as described in Section 2.1, apply here as well. The schematic of the entire setup and the detailed descriptions are available elsewhere [47].

The oxidation experiments were performed at temperatures between 475 and 800 K at 100 atm. The nominal residence time was defined as the ratio of the reactor volume to the volume flow rate at the specific temperature and pressure. The inlet volume flow rate was fixed to reduce the error in flow control and perturbation. Therefore, the flow residence time of the experiment changed with the temperature. Each measurement was conducted at least twice to ensure the experimental repeatability [48].

3. Detailed chemical kinetic model

The chemical kinetic model consists of subsets for *n*-heptane, ammonia, and interactions between the amine and hydrocarbon species. The full mechanism and thermodynamic data are available as Supplementary Material. The *n*-heptane subset was drawn from Zhang et al. [20], since this mechanism provides the best overall agreement with high-pressure ignition delay and flow reactor experiments [22]. In the Zhang et al. scheme, the H_2-O_2 subset was replaced by the updated Princeton HP-Mech [43], which involves the most recent fitting of experimental results or theoretical calculations for several key reactions involving HO_2 chemistry. The H_2O_2 subset, including the singlet/triplet competing channels, was updated based the recent study of Klippenstein et al. [49]. The second channel (R2) of reaction

$$HO_2 + HO_2 \rightleftarrows H_2O_2 + O_2 \qquad (R1)$$

$$HO_2 + HO_2 \rightleftarrows 2OH + O_2 \qquad (R2)$$

introduced in Klippenstein et al. [49], enhances the intermediate temperature chemistry, especially for high pressure conditions.

The amine subset was adopted without change from Glarborg [44]. This part of the mechanism draws mainly on the review of nitrogen chemistry by Glarborg et al. [37], but includes updates for NH_2 + H (+M) [50,51], NH_3 + HO_2 [40], NH_2 + HO_2 [50,52], amine + NO_2 [44], and steps in the diazene subset [53].

An important objective of the present work was to establish a subset for the chemical coupling between the *n*-heptane and the amine chemistry. Of particular interest was the H-abstraction from *n*-heptane by NH_2,

$$n\text{-}C_7H_{16} + NH_2 \rightleftarrows C_7H_{15} + NH_3 \qquad (R3 - R6)$$

where the heptyl radical could be any of the four isomers (C_7H_{15}-(1,2,3,4)). Fuel + NH_2 type reactions are known to be of major importance for ignition of binary mixtures of ammonia with small hydrocarbon fuels [54–56]. The rate constants for (R3-R6) were estimated by analogy to similar reactions of smaller hydrocarbons. Siddique et al. [57,58] employed CBS-QB3 methodology and conventional TST to calculate rate constants for H-abstraction by NH_2 from different C-H sites for a number of aliphatic (up to C_4) and aromatic molecules. Their calculated total rate constants for C_3H_8 were shown to agree well with experimental values from Demissy and Lesclaux [59] (300–500 K), Ehbrecht et al. [60] (550–1070 K), and Hennig and Wagner [61] (1500–2100 K). Figure 1 shows the variation in the rate constant for primary and secondary alkyl radicals, as reported by Siddique et al. [57,58], together with the values calculated by Mebel and Lin [62].

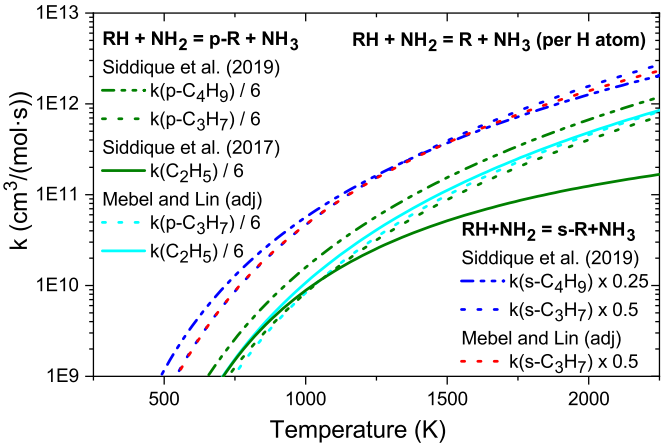

Fig. 1. Rate constant of the H-abstraction reaction by NH_2 forming primary and secondary alkyl radicals (per H atom): *p*-C_3H_7 and *s*-C_3H_7 (dotted lines) [58,62]; *p*-C_4H_9 and *s*-C_4H_9 (dash-dot-dot lines) [58] and C_2H_5 (solid lines) [57,62]. Note that Mebel and Lin [62] adjusted the theoretically calculated values within the method accuracy for better agreement with available experimental data.

In the present model, the values from Siddique et al. [57,58] were taken directly or extended by analogy, scaling for the correct degeneracy level, for all *n*-alkane and *n*-alkene molecules present in the mechanism. Rate constants for the *n*-heptane + NH_2 reaction are listed in Table 1. As discussed below, while predicted ignition delay times are very sensitive to the presence of the *n*-heptane + NH_2 reaction, the A-factor sensitivity is not substantial. For this reason, the uncertainty associated with using the analogy approach for this reaction is not expected to affect significantly the modeling predictions.

It is known that hydrocarbon/NO_x interactions may promote or inhibit reaction, dependent on the fuel and the reaction conditions [63]. Reaction classes include

$$ROO + NO \rightleftarrows RO + NO_2$$

$$ROO + NO(+M) \rightleftarrows RONO_2(+M)$$

$$RH + NO_2 \rightleftarrows R + HONO$$

Reactions of the type ROO + NO ⇄ RO + NO_2 may inhibit ignition of large hydrocarbons in systems with initial presence of NO [64]. Chen et al. [65] studied autoignition of *n*-heptane/NO mixtures and summarized hydrocarbon/NO submechanisms available in literature. In binary mixtures with NH_3, where no or little NO is present among the initial reactants, the hydrocarbon/NO_x interactions are expected to have lower importance, but we include them in the present model for completeness. Recommended values for methyl, ethyl-, *n*-propyl and *i*-propyl peroxy radicals with NO do not deviate from each other by more than 25% [66], and the rate constants for $C_7H_{15}OO$ + NO are estimated by analogy to CH_3O_2 + NO ⇄ CH_3O + NO_2. Formation of nitrate from $C_7H_{15}OO$ + NO (+M) is presumably insignificant at elevated temperatures and was not considered further. For the C_7H_{15}-3 + NO_2 reaction, the rate constants were adopted from the recent study of Almodovar and Goldsmith [67]; following Fang et al. [64], the other heptyl isomers

Table 1
Rate constants for the NH_2 + *n*-heptane reactions, as estimated in the present work. Parameters for use in the modified Arrhenius expression $k = AT^{\beta} \exp(-E/[RT])$. Units are mol, cm, s, cal.

		A	β	E	Source
(R3)	$n - C_7H_{16} + NH_2 \rightleftarrows C_7H_{15}\text{-}1 + NH_3$	1.8E00	3.880	4183	pw
(R4)	$n - C_7H_{16} + NH_2 \rightleftarrows C_7H_{15}\text{-}2 + NH_3$	8.2E01	3.370	3059	pw
(R5)	$n - C_7H_{16} + NH_2 \rightleftarrows C_7H_{15}\text{-}3 + NH_3$	8.2E01	3.370	3059	pw
(R6)	$n - C_7H_{16} + NH_2 \rightleftarrows C_7H_{15}\text{-}4 + NH_3$	4.1E01	3.370	3059	pw

were assumed to have analogous rate constants. Other reactions of the NO_x subset involving C_3–C_7 hydrocarbons were adopted from Fang et al. [64], but were found to be of low importance for the conditions of the present work. For the smaller hydrocarbons, the C/H/N/O subset was drawn from the review of Glarborg et al. [37].

4. Results and discussion

The revised NH_3/*n*-heptane mechanism has been validated by comparison with high-pressure experiments from literature (the ignition delay measurements from Yu et al. [23]) and from the present work. In addition to evaluating the predictive capabilities of the revised model at high pressure, the importance of the chemical coupling is discussed.

4.1. Ignition delay

Figure 2 presents simulations of ignition delay measurements in RCM of Yu et al. [23] for a selected case of a stoichiometric 90/10 (mole fraction) NH_3/*n*-heptane mixture at 15 bar, while results for mixtures containing 0–90% NH_3 are reported in the Supplementary Material (Figs. S2 and S3). In the modeling, volume profiles obtained by Yu et al. [23] from pressure histories, are implemented. First and main ignition events were determined at pressure inflection points, as done in the experiments [23]. The results of [23] are plotted with a ±15% uncertainty reported therein.

Predictions with the mechanism developed in the present work are compared to calculations with the model of Yu et al. [23] who merged the *n*-heptane model of Zhang et al. [20] with the mechanism of Glarborg et al. [37]. Even though we adopted a different merging approach in the present work, we found that combining the mechanisms of Zhang et al. and Glarborg et al. yielded predictions almost identical to those of Yu et al.

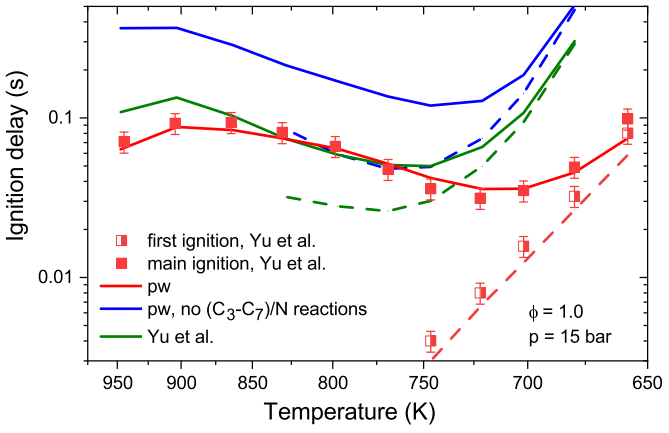

Fig. 2. Comparison of experimental (symbols, from Yu et al. [23]) and predicted (lines) ignition delay times for a fuel mixture of 9.6% *n*-heptane and 90.4% NH_3 in 10.5% O_2 and 88.5% Ar with a fuel-air equivalence ratio $\phi = 1$ and a pressure of 15 bar. Solid lines, filled symbols – main ignition; dashed lines, open symbols first ignition. Simulations using the measured RCM compression histories [23] were conducted with the model developed in the present work (red), with that excluding the C_3-C_7/N interaction subset (blue), and with the model of Yu et al. [23] (green). (For interpretation of the references to colour in this figure legend, the reader is referred to the web version of this article.)

The influence of the updated H_2/O_2 subset on ignition can be best viewed from the results for pure *n*-heptane (Fig. S2 in SM), where that subset is the difference between the present model and that of Yu et al. [23]. The present model predicts considerably faster ignition for *n*-heptane, compared to the mechanism by Yu et al. The observed differences are due to the addition of reaction (R2) from [49], as can be seen from Fig. S2(1), since by switching rate expressions of HO_2+HO_2 reaction, predictions of the present model become almost identical to the mechanism of Yu et al. [23]. The effect of (R1-R2) on ignition delay of *n*-heptane increases with temperature and is most pronounced at $T > 800$ K, in line with the results reported by Klippenstein et al. [49].

For the 90% NH_3 fuel mixture in Fig. 2, the present mechanism (red lines) closely follows the experimental results [23] in terms of both first and main ignition. The results are significantly improved compared to the merged model of Yu et al. [23] (green), which predicts a qualitatively different profile for the first ignition and overestimates both the main ignition at $T < 750$ K and the NTC initiation temperature.

In order to illustrate the influence of the updates in different subsets of the mechanism on ignition delay, predictions with the present mechanism without the interaction reactions between nitrogen-containing and C_3-C_7 species are shown as a blue curve in Fig. 2. It can be seen that the updates in the amine subset, primarily, the novel rate constant for the NH_2+HO_2 reaction [52], slow down the ignition, due to the significantly increased importance of the termination channel

$$NH_2 + HO_2 \rightleftarrows NH_3 + O_2 \quad \text{(R7)}$$

in the present mechanism, compared to the propagation channel

$$NH_2 + HO_2 \rightleftarrows H_2NO + OH \quad \text{(R8)}$$

in the mechanism of Glarborg et al. [37]. Still, the interval between the first and the main ignition, predicted by the "no C_3–C_7 interaction" mechanism, is comparable to that predicted by the mechanism of Yu et al. [23]. Inclusion of H-abstraction from *n*-heptane by NH_2 (R3–R6) into the interaction subset accelerates the initial *n*-heptane consumption, enhancing the first ignition and subsequently affecting the chemistry leading to the main ignition. Also for other NH_3/*n*-heptane mixtures (Figs. S2 and S3 in SM), good agreement between predictions with the present mechanism and the experimental results from Yu et al. was obtained. It can be concluded that the modifications in the different subsets of the mechanism were essential for correct prediction of ignition of NH_3/*n*-heptane binary mixtures.

4.2. High-pressure flow reactor results

The high pressure plug flow reactor experiments were conducted at both 21 bar and 100 bar, and stoichiometric and oxidizing conditions. The *n*-heptane/NH_3 molar ratio was maintained at 10%. An overview of the mixture compositions is provided

Table 2
Conditions for the flow reactor experiments.

Mixture	Pressure bar	ϕ	*n*-Heptane ppm	Ammonia ppm	Oxygen ppm
1	21	1.1	50.8	477	839
2	21	0.1	51.3	493	9215
3	100	1.1	49.5	488	858
4	100	0.1	50.5	510	9803

in Table 2, and details are given in Table S2 in Supplementary Material. The residence time in the isothermal zone, which depends on the temperature and pressure, is measured to be 6–10 s at 21 bar and 28–57 s at 100 bar. The model predictions are conducted using Chemkin Pro by ANSYS v.19.1 [68] by assuming plug flow conditions in the reactor and including the whole temperature profile presented in Fig. S1 in the Supplementary Material.

The measured NH_3 and *n*-heptane mole fractions are compared with modeling predictions in Fig. 3. Uncertainties associated with the GC measurements are displayed as error bars. Predictions are shown for both the present mechanism (solid lines) and the mechanism by Yu et al. [23] (dashed lines). The conversion of *n*-heptane exhibits a low temperature region from 500 K to 700 K and a high temperature region above 700 K. An increase in pressure or O_2 level promotes the low temperature *n*-heptane conversion and lowers the onset temperature. A pronounced NTC region is only observed at 21 bar and stoichiometric conditions, whereas at higher oxygen levels and/or higher pressure, a transition region is detected as a plateau in the *n*-heptane mole fraction. Low temperature conversion of NH_3 is only observed at high pressure and lean conditions. At 100 bar and stoichiometric conditions, as well as at 21 bar and lean conditions, the NH_3 conversion has an onset temperature of 700 K, coinciding with the high temperature onset of *n*-heptane oxidation. For 21 bar and stoichiometric conditions, no NH_3 conversion is observed. The increasing levels of NH_3 observed in the low temperature region and just before the full conversion of *n*-heptane for the conditions at 21 bar, and 100 bar stoichiometric, is assumed to be an analyzer cross interference with some of intermediates formed in the *n*-heptane oxidation. Pure ammonia oxidation at similar conditions have previously been conducted with the setup [21], and the ammonia increase has only been observed in mixtures with *n*-heptane, thus, indicating a cross interference in the analyzer.

Comparison of the present results with previous high-pressure flow reactor studies on ammonia [21] and *n*-heptane [22] allows an assessment of the mutual interaction between the two fuels. The presence of *n*-heptane lowers the onset temperature for ammonia about 100 K compared to pure NH_3 oxidation under similar conditions. The promoting effect of *n*-heptane is consistent with reported ignition delay measurements. For *n*-heptane, the oxidation behavior with a low temperature region of roughly 500–700 K and high temperature region starting at 700 K is the same with and without presence of NH_3. However, ammonia addition has an inhibiting effect on the low temperature *n*-heptane oxidation; the conversion in the NTC region is reduced by a factor of two, and the onset temperature is increased by up to 50 K.

The present model provides a satisfactory prediction of the *n*-heptane and ammonia profiles. The NTC behavior for *n*-heptane at lean conditions and 21 bar is captured, even though the width of this region is slightly underpredicted. The main discrepancy is the overprediction of the NH_3 conversion at higher temperatures for lean conditions at 21 bar.

Predictions with the model from Yu et al. [23] are less accurate. Notably, this model does not predict NTC behavior for *n*-heptane at lean conditions and 21 bar. This discrepancy can be attributed mostly to the failure to describe direct interactions between the

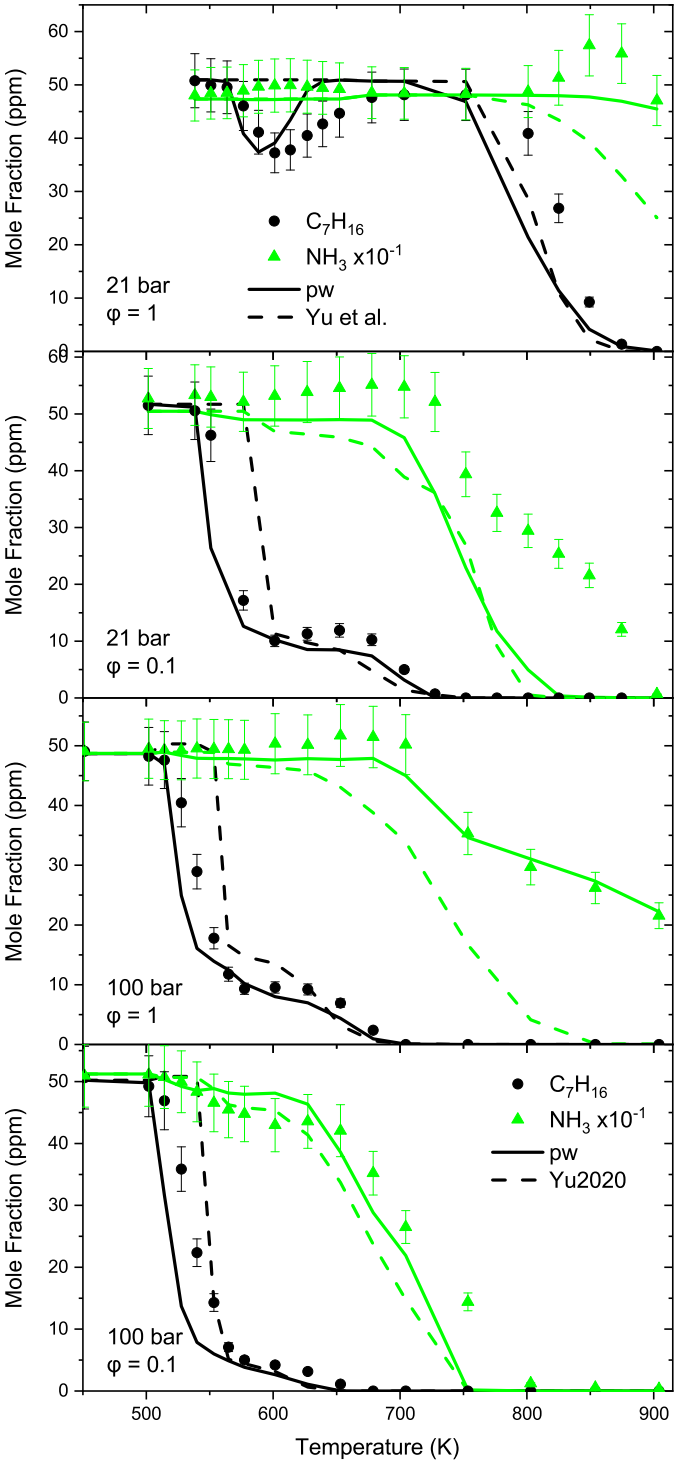

Fig. 3. Comparison of measured and predicted mole fractions of *n*-heptane and ammonia in oxidation of a NH_3/*n*-heptane mixture at high-pressure flow reactor conditions. Experimental results are shown as symbols. Modeling predictions are shown as solid lines (present model) or dashed lines (model from Yu et al. [23]). The residence times in the isothermal zone are 6–10 s at 21 bar and 28–57 s at 100 bar, decreasing with temperature. Mixture compositions are listed in Table 2.

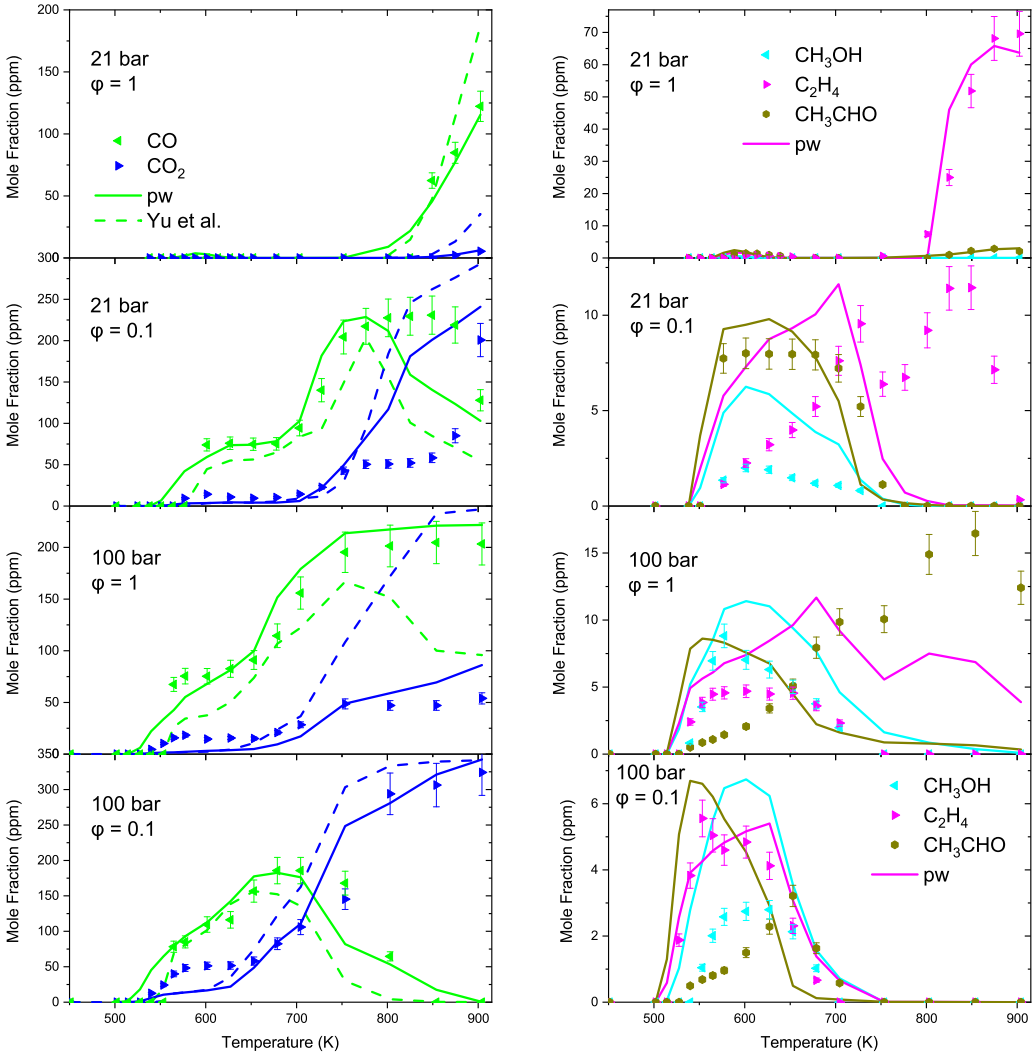

Fig. 4. CO, CO_2, methanol, ethene and acetaldehyde mole fractions measured in the NH_3/*n*-heptane mixture oxidation at given conditions in the plug flow reactor experiments. The residence times are 6–10 s at 21 bar and 28–57 s at 100 bar, in the isothermal zone, decreasing with temperature. Mixture compositions are given in Table 2. Symbols: experimental results. Lines: model predictions by the present model and Yu et al. [23].

ammonia and *n*-heptane, in particular omission of the reaction between NH_2 and *n*-heptane (R3–R6). The model from Yu et al. also tends to overpredict the reactivity of ammonia at higher temperatures. The improved performance of the present model in terms of NH_3 consumption is facilitated by the updates in the amine subset compared to Glarborg et al. [37], mainly the use of the recent theoretical rate constants for NH_2 + HO_2 from Klippenstein and Glarborg [52].

Comparisons of measured mole fractions of CO and CO_2, and intermediates such as methanol, ethene, acetaldehyde with modeling predictions are shown in Fig. 4. Similar comparisons for O_2 and minor intermediates are shown in Fig. S4 in the Supplementary Material, along with calculations made with the Yu et al. model. It is difficult to close a carbon balance as the GC is not calibrated for all intermediates in *n*-heptane oxidation. However, at high O_2 levels carbon balances within 90% at the highest temperature (see also Fig. S5 in the Supplementary Material).

Formation of CO and CO_2 is restricted to conditions where most of the *n*-heptane has been consumed. No CO/CO_2 is formed in the NTC region at 21 bar/stoichiometric, but carbon oxides are detected in the transition region at higher O_2/pressure; most pronounced at 21 bar fuel lean conditions and 100 bar stoichiometric conditions where they form a plateau.

The model generally provides a good prediction of CO and CO_2, except for the 21 bar/lean mixture, where CO oxidation is overpredicted at high temperatures. Compared to the model of Yu et al., the present model has better predictions at all conditions; especially at 100 bar stoichiometric conditions the model predictions are vastly improved.

Acetaldehyde and methanol are mainly formed in the low temperature oxidation as they are products of the decomposition of keto-hydroperoxides [22]. Ethene is mainly formed in the high temperature region as it is a main product of the thermal decomposition of heptyl radicals. The ethene formation is most pronounced at 21 bar stoichiometric conditions where the thermal decomposition is favoured. However, at 100 bar lean conditions all the hydrocarbons are oxidized to CO_2 at higher temperatures.

The predictions of the intermediates are controlled by the *n*-heptane subset; however, the model updates do have a minor impact on the calculations. Both the present model and that of Yu et al. predict the trend of low temperature formation of acetaldehyde, methanol, and ethene (see SM), but neither mechanism captures the high temperature formation of ethane. In line with the findings of Thorsen et al. [22] for pure *n*-heptane as fuel, model improvements for the *n*-heptane subset are required to properly predict the intermediate species mole fractions.

Table 3
Conditions for the jet-stirred reactor experiments.

Mixture	Pressure bar	ϕ	*n*-Heptane ppm	Ammonia ppm	Oxygen %
1	100	0.1	400	4000	7.4
2	100	1.0	400	4000	0.74

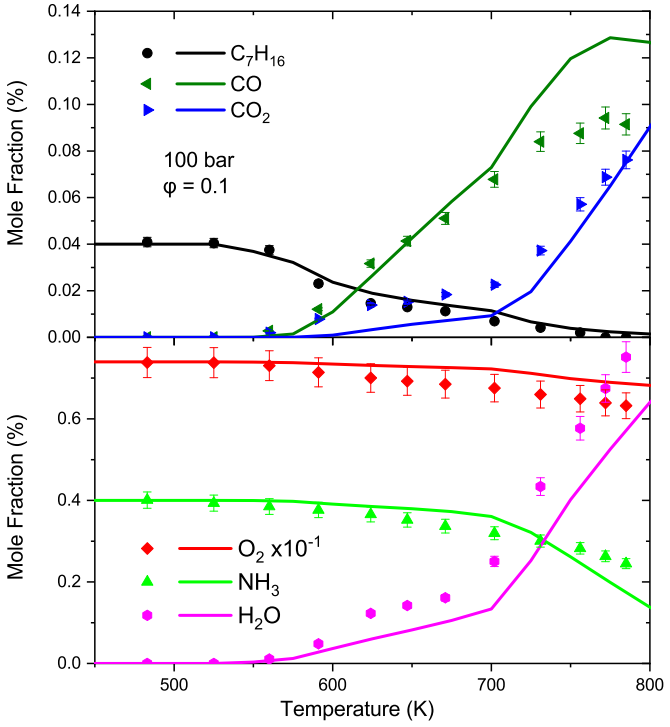

Fig. 5. Comparison of measured and predicted mole fractions in oxidation of a fuel-lean (ϕ = 0.1) NH_3/*n*-heptane mixture at 100 atm in a jet-stirred reactor. Experimental results are shown as symbols and modeling predictions with the present model are shown as solid lines. The mixture composition is listed in Table 3.

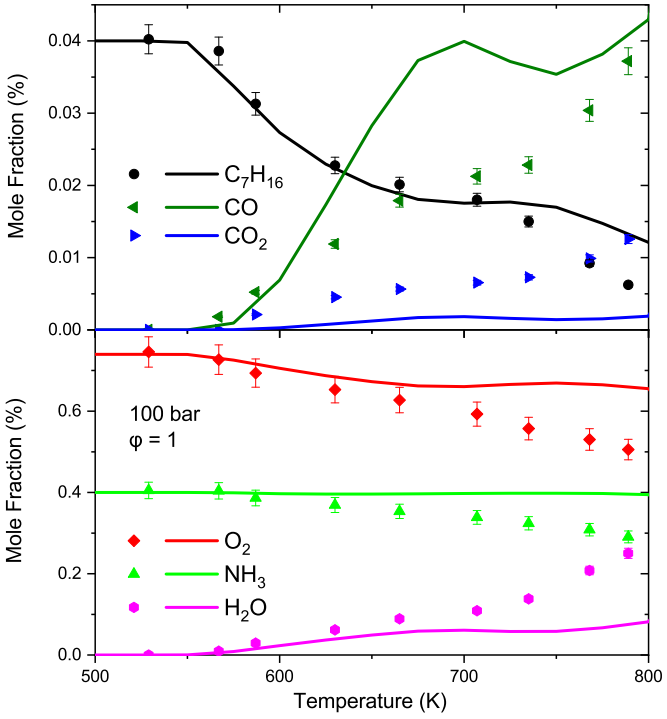

Fig. 6. Comparison of measured and predicted mole fractions in oxidation of a stoichiometric (ϕ = 1.0) NH_3/*n*-heptane mixture at 100 atm in a jet-stirred reactor. Experimental results are shown as symbols and modeling predictions with the present model are shown as solid lines. The mixture composition is listed in Table 3.

4.3. Supercritical pressure jet-stirred reactor results

The supercritical pressure jet-stirred reactor (SP-JSR) experiments were conducted at 100 atm, and fuel-air equivalence ratios of 0.1 and 1.0. The inlet flow rate in both cases was fixed, corresponding to residence times of 0.50–0.30 s (475–800 K). The *n*-heptane/NH_3 ratio was maintained at 10%. The mixture compositions are listed in Table 3. Simulation of the experimental results was performed with the transient PSR reactor model in Chemkin at constant temperature.

Figure 5 shows a comparison of measured and predicted mole fractions of major species as a function of temperature. Similarly to Figs. 3 and 4, uncertainty of the μ-GC measurements is shown here as error bars. The experimental results show that *n*-heptane starts to be oxidized at a temperature around 550 K. The consumption of NH_3 is initiated around 600 K, significantly below the onset temperature for pure NH_3 oxidation. This can be explained by the active radicals produced by the low temperature oxidation of *n*-heptane. Similar to the flow reactor results discussed above, the experimental *n*-heptane mole fraction profile exhibits a narrow shoulder, here from 625 to 700 K. The plateau represents the remnant of the negative temperature coefficient (NTC) behavior, where the *n*-heptane consumption slows down with increasing temperature. The species profiles for CO_2 and H_2O in Fig. 5 also exhibit a shoulder in the same temperature region as the *n*-heptane profile.

The modeling predictions show good agreement with experimental data, especially for *n*-heptane. However, the model slightly overpredicts NH_3 at lower temperatures, while it underpredicts NH_3 in the intermediate temperature region. The increased OH radical production via the H_2O_2 (+M) ⇄ 2OH (+M) and $2HO_2$ ⇄ 2OH + O_2 reactions at high pressure shifts the intermediate temperature chemistry to lower temperature.

Figure 6 compares measured and predicted species mole fractions for an equivalence ratio of 1.0. The onset temperatures for oxidation of *n*-heptane and NH_3 are slightly higher than for the fuel-lean mixture, since a decrease in the O_2 level inhibits the low temperature oxidation of *n*-heptane and NH_3. The experimental species profiles exhibit a transition region under stoichiometric conditions, consistent with the observations for the fuel-lean mixture. The intermediate temperature oxidation becomes weaker at stoichiometric conditions compared to that at fuel-lean conditions due to the lack of O_2 resulting in comparatively less peroxide formation.

The model predicts well the *n*-heptane profile at low temperatures, but at intermediate temperatures the consumption is underpredicted. The model also underpredicts the NH_3 consumption as well as formation of H_2O and CO_2, while it overpredicts CO. The reason for this difference is not known at present. Wang et al. [69] observed similar differences in modeling high-pressure methanol oxidation, and suggested that reactions involving CO or HCO, such as CO + OH ⇄ CO_2 + H, CO + HO_2 ⇄ CO_2 + OH, HCO + HO_2 ⇄ H + OH + CO_2, and HCO (+M) ⇄ H + CO (+M) need further consideration for extremely high pressure. However, the

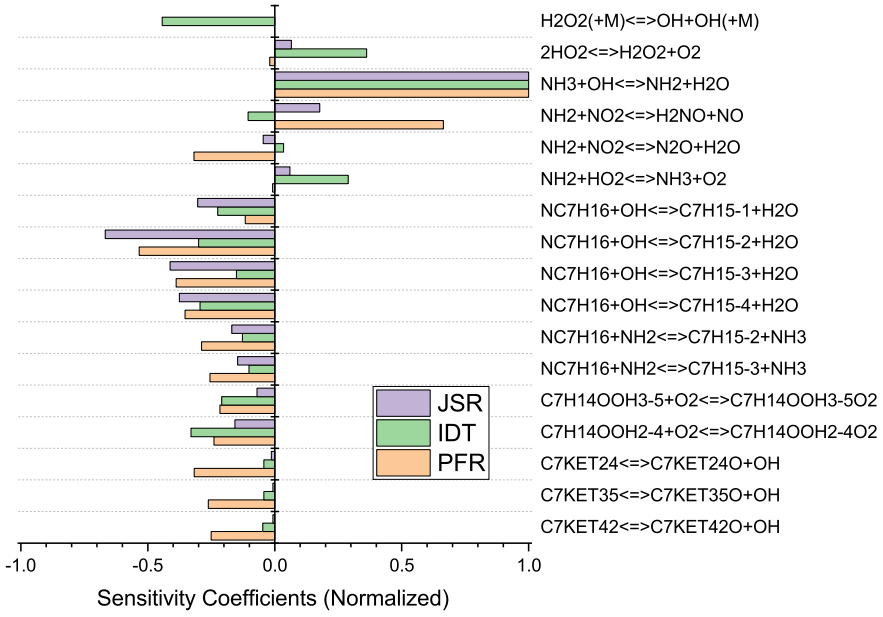

Fig. 7. Sensitivity coefficients for the ignition delay time or concentration of *n*-heptane in jet-stirred reactor and plug flow calculations. Conditions used in the calculations are 15 bar and 700 K for IDT, 100 bar and 650 K for JSR, and 100 bar and the 528 K temperature profile for PFR. The conditions are chosen to have around 50% *n*-heptane conversion.

NH_3/*n*-heptane oxidation chemistry is more complex than that of methanol and more work is required to resolve this issue.

4.4. Reaction path and sensitivity analysis

A detailed reaction path diagram for oxidation of *n*-heptane is shown in the Supporting Material for stoichiometric conditions (21 bar and 601 K or 903 K). *n*-Heptane is consumed by reaction with OH and NH_2. The major low temperature pathway is through hydrogen abstraction on the second position, forming C_7H_{15}-2, followed by cyclic ether formation. Formation of cyclic ether is favored over the chain-branching pathway through keto-hydroperoxide (OQOOH) for all C_7H_{15} isomers except C_7H_{15}-4. This is consistent with results for pure *n*-heptane oxidation [22]. However, the presence of NH_3 promotes the keto-hydroperoxide pathway compared to the oxidation of pure *n*-heptane. The major high temperature reaction pathway also involves C_7H_{15}-2, which decomposes thermally into ethene. Comparing the high temperature oxidation of pure *n*-heptane [22] and NH_3/*n*-heptane, no notable differences are observed.

Figure 7 shows a sensitivity analysis for the ignition delay time in RCM or concentration of *n*-heptane in jet-stirred reactor and plug flow calculations. Negative sensitivity coefficients indicate a reaction that promotes ignition or oxidation of *n*-heptane, while positive coefficients indicate an inhibiting step. The sensitivity analysis shows that the low temperature initiation is promoted by the hydrogen abstraction from *n*-heptane by OH and NH_2. Also the second addition of O_2 and the decomposition of keto-hydroperoxides enhance reaction, emphasizing the importance of the chain branching pathway. The reaction sequence NH_3 + OH $\rightleftarrows$ NH_2 + H_2O, NH_2 + HO_2 $\rightleftarrows$ NH_3 + O_2 is chain terminating and both reactions exhibit positive sensitivity coefficients. The sequence competes with H-abstraction from *n*-heptane by OH and NH_2; it is responsible for the inhibiting effect of NH_3 on *n*-heptane oxidation.

While addition of H-abstraction from *n*-heptane by NH_2 (R3-R6) was necessary for reproduction of the experimental results, the A-factor sensitivity for this reaction is not large, especially for IDT, as this chain-propagation reaction is not rate-limiting. This confirms the adequacy of the analogy approach to determination of rate constant of this reaction.

The NH_2 + NO_2 reaction shows up as important, either enhancing or inhibiting oxidation depending on the products. The H_2O_2 chemistry is mainly important for the IDT calculations, where HO_2 + HO_2 $\rightleftarrows$ H_2O_2 + O_2 is chain-terminating while H_2O_2(+M) $\rightleftarrows$ OH + OH (+M) enhances reaction. The JSR and PFR calculations are less sensitive to this subset. At low temperatures, predictions are also sensitive to the thermal dissociation of the ROO radical, which forms HO_2 and an alkene, while at elevated temperature reactions involving CH_3 and HO_2 radicals become more important, as observed also for *n*-heptane oxidation [22].

5. Conclusions

In the present work, experiments using a high-pressure flow reactor and a supercritical pressure jet stirred reactor were performed to study co-oxidation of NH_3 and *n*-heptane, a binary mixture relevant for practical combustion devices, and to provide experimental data at pressures up to 100 atm, conditions that have not been accessed previously. The results were interpreted using a detailed chemical kinetic model for ignition and oxidation of NH_3/*n*-heptane mixtures at high pressure, developed as part of this work. The oxidation of a 90/10 NH_3/*n*-heptane mixture (by mole fraction) was characterized experimentally in a laminar flow reactor and a jet-stirred reactor at pressures of 20–100 atm and temperatures of 400–900 K. In addition, ignition delay times measured in a rapid compression machine by Yu et al. [23] were included in the analysis. The kinetic mechanism introduces a subset for the chemical coupling between nitrogen-containing species and heavy hydrocarbons, with particular emphasis on the NH_2 + *n*-C_7H_{16} reaction. The rate constants were obtained from data for other hydrocarbons, by adopting analogy rules. In addition, the present mechanism includes recently updated hydrogen [43] and amine [44] subsets. The updates in HO_2 reactions, i.e., HO_2+HO_2 in the hydrogen subset, and NH_2+HO_2 in the amine subset, respectively, were of particular importance for the studied conditions. The kinetic model provided a good prediction of the ignition delay times by Yu et al. [23] as well as the high pressure experimental data

obtained in the present work. The results show the importance of including updated rate constants for NH_2+HO_2 and NH_2 + n-C_7H_{16} to obtain reliable predictions for ignition and oxidation of NH_3/n-heptane mixtures at high pressure, as they affect the simulation results qualitatively. The updates in the H_2 submechanism have a quantitative effect on ignition in the intermediate temperature range. The effectiveness of the analogy approach to determination of the rate constants in the interaction subset was confirmed by the observed results.

Declaration of Competing Interest

The authors declare that they have no known competing financial interests or personal relationships that could have appeared to influence the work reported in this paper.

Acknowledgments

VA, EN and PG would like to acknowledge that their contribution is part of the project ENGIMMONIA that has received funding from the European Research Council (ERC) under the European Union's Horizon 2020 research and innovation program (Grant agreement no. 955413). PG would like to thank also for the support from Innovation Fund Denmark for the AEngine Grand Solutions project. YJ would like to thank the DOE for the grant support of DE-SC0021135.

Supplementary material

Supplementary material associated with this article can be found, in the online version, at doi:10.1016/j.combustflame.2023.112785.

References

[1] A. Valera-Medina, H. Xiao, M. Owen-Jones, W.I.F. David, P.J. Bowen, Ammonia for power, Prog. Energy Combust. Sci. 69 (2018) 63–102.
[2] H. Kobayashi, A. Hayakawa, K.K.A. Somarathne, E.C. Okafor, Science and technology of ammonia combustion, Proc. Combust. Inst. 37 (2019) 109–133.
[3] A. Valera-Medina, F. Amer-Hatem, A.K. Azad, I. Dedoussi, M. De Joannon, R.X. Fernandes, P. Glarborg, H. Hashemi, X. He, S. Mashruk, J. McGowan, C. Mounaim-Rouselle, A. Ortiz-Prado, J.A. Ortiz-Valera, I. Rossetti, B. Shu, M. Yehia, H. Xiao, M. Costa, A review on ammonia as a potential fuel: from synthesis to economics, Energy Fuels 35 (2021) 6964–7029.
[4] W.S. Chai, Y. Bao, P. Jin, G. Tang, L. Zhou, A review on ammonia, ammonia-hydrogen and ammonia-methane fuels, Renew. Sustain. Energy Rev. 147 (2021) 111254.
[5] A.J. Reiter, S.C. Kong, Combustion and emissions characteristics of compression-ignition engine using dual ammonia-diesel fuel, Fuel 90 (2011) 87–97.
[6] Y. Niki, Y. Nitta, H. Sekiguchi, K. Hirata, Diesel fuel multiple injection effects on emission characteristics of diesel engine mixed ammonia gas into intake air, J. Eng. Gas Turbines Power 141 (2019) 061020.
[7] P. Dimitriou, R. Javaid, A review of ammonia as a compression ignition engine fuel, Int. J. Hydrogen Energy 45 (2020) 7098–7118.
[8] A. Yousefi, H. Guo, S. Dev, S. Lafrance, B. Liko, A study on split diesel injection on thermal efficiency and emissions of an ammonia/diesel dual-fuel engine, Fuel 316 (2022) 123412.
[9] A. Yousefi, H. Guo, S. Dev, B. Liko, S. Lafrance, Effects of ammonia energy fraction and diesel injection timing on combustion and emissions of an ammonia/diesel dual-fuel engine, Fuel 314 (2022) 122723.
[10] V. Scharl, T. Sattelmayer, Ignition and combustion characteristics of diesel piloted ammonia injections, Fuel Commun. 11 (2022) 100068.
[11] Y. Feng, J. Zhu, Y. Mao, M. Raza, Y. Qian, L. Yu, X. Lu, Low-temperature auto-ignition characteristics of NH_3/diesel binary fuel: ignition delay time measurement and kinetic analysis, Fuel 281 (2020) 118761.
[12] Y. Zhang, W. Zhou, Y. Liang, L. Yu, X. Lu, An experimental and detailed kinetic modeling study of the auto-ignition of NH_3/diesel mixtures: part 1- NH_3 substitution ratio from 20% to 90%, Combust. Flame (2022) 112391, doi:10.1016/j.combustflame.2022.112391.
[13] O. Mathieu, E.L. Petersen, Experimental and modeling study on the high-temperature oxidation of ammonia and related NO_x chemistry, Combust. Flame 162 (2015) 554–570.
[14] X. He, B. Shu, D. Nascimento, K. Moshammer, M. Costa, R.X. Fernandes, Auto-ignition kinetics of ammonia and ammonia/hydrogen mixtures at intermediate temperatures and high pressures, Combust. Flame 206 (2019) 189–200.
[15] M. Pochet, V. Dias, B. Moreau, F. Foucher, H. Jeanmart, F. Contino, Experimental and numerical study, under LTC conditions, of ammonia ignition delay with and without hydrogen addition, Proc. Combust. Inst. 37 (2019) 621–629.
[16] L. Dai, S. Gersen, P. Glarborg, H. Levinsky, A. Mokhov, Experimental and numerical analysis of the autoignition behavior of NH_3 and NH_3/H_2 mixtures at high pressure, Combust. Flame 215 (2020) 134–144.
[17] H.K. Ciezki, G. Adomeit, Shock-tube investigation of self-ignition of n-heptane-air mixtures under engine relevant conditions, Combust. Flame 93 (1993) 421–433.
[18] K. Fieweger, R. Blumenthal, G. Adomeit, Shock-tube investigations on the self-ignition of hydrocarbon-air mixtures at high pressures, Symp. (Int.) Combust. 25 (1994) 1579–1585.
[19] K.A. Heufer, H. Olivier, Determination of ignition delay times of different hydrocarbons in a new high pressure shock tube, Shock Waves 20 (2010) 307–316.
[20] K. Zhang, C. Banyon, J. Bugler, H.J. Curran, A. Rodriguez, O. Herbinet, F. Battin-Leclerc, C. B'Chir, K.A. Heufer, An updated experimental and kinetic modeling study of n-heptane oxidation, Combust. Flame 172 (2016) 116–135.
[21] Y. Song, H. Hashemi, J.M. Christensen, C. Zou, P. Marshall, P. Glarborg, Ammonia oxidation at high pressure, Fuel 181 (2016) 358–365.
[22] L.S. Thorsen, M.S.T. Jensen, M.S. Pullich, J.M. Christensen, H. Hashemi, P. Glarborg, n-Heptane oxidation in a high pressure flow reactor, Int. J. Chem. Kinet. 54 (2022) 669–678.
[23] L. Yu, W. Zhou, Y. Feng, W. Wang, J. Zhu, Y. Qian, X. Lu, The effect of ammonia addition on the low-temperature autoignition of n-heptane: an experimental and modeling study, Combust. Flame 217 (2020) 4–11.
[24] M. Lubrano Lavadera, X. Han, A.A. Konnov, Comparative effect of ammonia addition on the laminar burning velocities of methane, n-heptane, and iso-octane, Energy Fuels 35 (2021) 7156–7168.
[25] J. Pan, R. Tang, Z. Wang, J. Gao, Q. Xu, G. Shu, H. Wei, An experimental and modeling study on the oxidation of ammonia and n-heptane with JSR, Proc. Combust. Inst. 39 (2023), doi:10.1016/j.proci.2022.07.193.
[26] M. Mehl, W.J. Pitz, C.K. Westbrook, H.J. Curran, Kinetic modeling of gasoline surrogate components and mixtures under engine conditions, Proc. Combust. Inst. 33 (2011) 193–200.
[27] L. Seidel, K. Moshammer, X. Wang, T. Zeuch, K. Kohse-Höinghaus, F. Mauss, Comprehensive kinetic modeling and experimental study of a fuel-rich, premixed n-heptane flame, Combust. Flame 162 (2015) 2045–2058.
[28] L. Cai, H. Pitsch, Optimized chemical mechanism for combustion of gasoline surrogate fuels, Combust. Flame 162 (2015) 1623–1637.
[29] E. Ranzi, C. Cavallotti, A. Cuoci, A. Frassoldati, M. Pelucchi, T. Faravelli, New reaction classes in the kinetic modeling of low temperature oxidation of n-alkanes, Combust. Flame 162 (2015) 1679–1691.
[30] Y. Wu, S. Panigrahy, A.B. Sahu, C. Bariki, J. Beeckmann, J. Liang, A.A.E. Mohamed, S. Dong, C. Tang, H. Pitsch, Z. Huang, H.J. Curran, Understanding the antagonistic effect of methanol as a component in surrogate fuel models: a case study of methanol/n-heptane mixtures, Combust. Flame 226 (2021) 229–242.
[31] L. Thorsen, C. Nordhjort, H. Hashemi, K.M. Pang, P. Glarborg, Evaluation of a semiglobal approach for modeling methane/n-heptane dual-fuel ignition, Energy Fuels 35 (17) (2021) 14042–14050, doi:10.1021/acs.energyfuels.1c01775.
[32] H.K. Ciezki, G. Adomeit, Shock-tube investigation of self-ignition of n-heptane-air mixtures under engine relevant conditions, Combust. Flame 93 (4) (1993) 421–433, doi:10.1016/0010-2180(93)90142-P.
[33] B.M. Gauthier, D.F. Davidson, R.K. Hanson, Shock tube determination of ignition delay times in full-blend and surrogate fuel mixtures, Combust. Flame 139 (4) (2004) 300–311, doi:10.1016/j.combustflame.2004.08.015.
[34] H.-P.S. Shen, J. Steinberg, J. Vanderover, M.A. Oehlschlaeger, A shock tube study of the ignition of n-heptane, n-decane, n-dodecane, and n-tetradecane at elevated pressures, Energy Fuels 23 (5) (2009) 2482–2489, doi:10.1021/ef8011036.
[35] J. Li, H. Huang, N. Kobayashi, C. Wang, H. Yuan, Numerical study on laminar burning velocity and ignition delay time of ammonia flame with hydrogen addition, Energy 126 (2017) 796–809.
[36] J. Otomo, M. Koshi, T. Mitsumori, H. Iwasaki, K. Yamada, Chemical kinetic modeling of ammonia oxidation with improved reaction mechanism for ammonia/air and ammonia/hydrogen/air combustion, Int. J. Hydrogen Energy 43 (2018) 3004–3014.
[37] P. Glarborg, J.A. Miller, B. Ruscic, S.J. Klippenstein, Modeling nitrogen chemistry in combustion, Prog. Energy Combust. Sci. 67 (2018) 31–68.
[38] B. Mei, X. Zhang, S. Ma, M. Cui, H. Guo, Z. Cao, Y. Li, Experimental and kinetic modeling investigation on the laminar flame propagation of ammonia under oxygen enrichment and elevated pressure conditions, Combust. Flame 210 (2019) 236–246.
[39] B. Mei, J. Zhang, X. Shi, Z. Xi, Y. Li, Enhancement of ammonia combustion with partial fuel cracking strategy: laminar flame propagation and kinetic modeling investigation of NH_3/H_2/N_2/air mixtures up to 10 atm, Combust. Flame 231 (2021) 111472.
[40] A. Stagni, C. Cavallotti, S. Arunthanayothin, Y. Song, O. Herbinet, F. Battin-Leclerc, T. Faravelli, An experimental, theoretical and kinetic-modeling study of the gas-phase oxidation of ammonia, React. Chem. Eng. 5 (2020) 696–711.
[41] Y. Jiang, A. Gruber, K. Seshadri, F. Williams, An updated short chemical-kinetic nitrogen mechanism for carbon-free combustion applications, Int. J. Energy Res. 44 (2020) 795–810.
[42] M. Pelucchi, M. Bissoli, C. Cavallotti, A. Cuoci, T. Faravelli, A. Frassoldati, E. Ranzi, A. Stagni, Improved kinetic model of the low-temperature oxidation of n-heptane, Energy Fuels 28 (2014) 7178–7193.

[43] H. Zhao, C. Yan, Z. Wang, A.W. Jasper, S.J. Klippenstein, Y. Ju, High-pressure hydrogen oxidation in N_2, CO_2, and H_2O dilutions up to 100 atm in a supercritical-pressure jet-stirred reactor, in preparation, 2022.
[44] P. Glarborg, The $NH_3/NO_2/O_2$ system: constraining key steps in ammonia ignition and N_2O formation, Combust. Flame (2022), doi:10.1016/j.combustflame.2022.112311.
[45] C.L. Rasmussen, J. Hansen, P. Marshall, P. Glarborg, Experimental measurements and kinetic modeling of $CO/H_2/O_2/NO_x$ conversion at high pressure, Int. J. Chem. Kin. 40 (2008) 454–480.
[46] H. Hashemi, J.M. Christensen, L.B. Harding, S.J. Klippenstein, P. Glarborg, High–pressure oxidation of propane, Proc. Combust. Inst. 37 (2019) 461–468.
[47] H. Zhao, C. Yan, T. Zhang, G. Ma, M.J. Souza, C.-w. Zhou, Y. Ju, Studies of high-pressure *n*-butane oxidation with CO_2 dilution up to 100 atm using a supercritical-pressure jet-stirred reactor, Proc. Combust. Inst. 38 (2021) 279–287.
[48] C. Yan, H. Zhao, Z. Wang, G. Song, Y. Lin, C.R. Mulvihill, A.W. Jasper, S.J. Klippenstein, Y. Ju, Low- and intermediate-temperature oxidation of dimethyl ether up to 100 atm in a supercritical pressure jet-stirred reactor, Combust. Flame 243 (2022) 112059.
[49] S.J. Klippenstein, R. Sivaramakrishnan, U. Burke, K.P. Somers, H.J. Curran, L. Cai, H. Pitsch, M. Pelucchi, T. Faravelli, P. Glarborg, $HO_2 + HO_2$: high level theory and the role of singlet channels, Combust. Flame 243 (2022) 111975.
[50] P. Glarborg, H. Hashemi, S. Cheskis, A.W. Jasper, On the rate constant for $NH_2 + HO_2$ and third-body collision efficiencies for $NH_2 + H$ (+ M) and $NH_2 + NH_2$ (+ M), J. Phys. Chem. A 125 (2021) 1505–1516.
[51] P. Glarborg, H. Hashemi, P. Marshall, Challenges in kinetic modeling of ammonia pyrolysis, Fuel Commun. 10 (2022) 100049.
[52] S.J. Klippenstein, P. Glarborg, Theoretical kinetics predictions for $NH_2 + HO_2$, Combust. Flame 236 (2022) 111787.
[53] P. Marshall, G. Rawling, P. Glarborg, New reactions of diazene and related species for modelling combustion of amine fuels, Mol. Phys. 119 (2021) e1979674.
[54] L. Dai, S. Gersen, P. Glarborg, A. Mokhov, H. Levinsky, Autoignition studies of NH_3/CH_4 mixtures at high pressure, Combust. Flame 218 (2020) 19–26.
[55] L. Dai, H. Hashemi, P. Glarborg, S. Gersen, P. Marshall, A. Mokhov, H. Levinsky, Ignition delay times of NH_3/DME blends at high pressure and low DME fraction: RCM experiments and simulations, Combust. Flame 227 (2021) 120–134.
[56] G. Issayev, B.R. Giri, A.M. Elbaz, K.P. Shrestha, F. Mauss, W.L. Roberts, A. Farooq, Ignition delay time and laminar flame speed measurements of ammonia blended with dimethyl ether: a promising low carbon fuel blend, Renew. Energy 181 (2022) 1353–1370.
[57] K. Siddique, M. Altarawneh, J. Gore, P.R. Westmoreland, B.Z. Dlugogorski, Hydrogen abstraction from hydrocarbons by NH_2, J. Phys. Chem. A 121 (2017) 2221–2231.
[58] K. Siddique, M. Altarawneh, A. Saeed, Z. Zeng, J. Gore, B.Z. Dlugogorski, Interaction of NH_2 radical with alkylbenzenes, Combust. Flame 200 (2019) 85–96.
[59] M. Demissy, R. Lesclaux, Kinetics of hydrogen abstraction by NH_2 radicals from alkanes in the gas-phase - a flash-photolysis laser resonance-absorption study, J. Am. Chem. Soc. 102 (1980) 2897–2902.
[60] J. Ehbrecht, W. Hack, P. Rouveirolles, H.G. Wagner, Hydrogen abstraction reactions by NH_2-radicals from hydrocarbons in the gas-phase, Ber. Bunsen. Phys. Chem. 91 (1987) 700–708.
[61] G. Hennig, H.G. Wagner, A kinetic study about the reactions of NH_2 radicals with saturated- hydrocarbons in the gas-phase, Ber. Bunsen. Phys. Chem. 99 (1995) 863–869.
[62] A.M. Mebel, M.C. Lin, Prediction of absolute rate constants for the reactions of NH_2 with alkanes from ab initio G2M/TST calculations, J. Phys. Chem. A 103 (1999) 2088–2096.
[63] P. Glarborg, Hidden interactions—Trace species governing combustion and emissions, Proc. Combust. Inst. 31 (2007) 77–98.
[64] R. Fang, C. Saggese, S.W. Wagnon, A.B. Sahu, H.J. Curran, W.J. Pitz, C.J. Sung, Effect of nitric oxide and exhaust gases on gasoline surrogate autoignition: iso-octane experiments and modeling, Combust. Flame 236 (2022) 111807.
[65] Z. Chen, P. Zhang, Y. Yang, M.J. Brear, X. He, Z. Wang, Impact of nitric oxide (NO) on *n*-heptane autoignition in a rapid compression machine, Combust. Flame 186 (2017) 94–104.
[66] R. Atkinson, D.L. Baulch, R.A. Cox, J.N. Crowley, R.F. Hampson, R.G. Hynes, M.E. Jenkin, M.J. Rossi, J. Troe, Evaluated kinetic and photochemical data for atmospheric chemistry: volume II–gas phase reactions of organic species, Atm. Chem. Phys. 6 (2006) 3625–4055.
[67] C.A. Almodovar, C.F. Goldsmith, Laser schlieren study of the thermal decomposition of 2-ethylhexyl-nitrate, Proc. Combust. Inst. 38 (2021) 997–1005.
[68] ANSYS, Inc., ANSYS 19.1 Chemkin-Pro, 2018.
[69] Z. Wang, H. Zhao, C. Yan, Y. Lin, A.D. Lele, W. Xu, B. Rotavera, A.W. Jasper, S.J. Klippenstein, Y. Ju, Methanol oxidation up to 100 atm in a supercritical pressure jet-stirred reactor, Proc. Combust. Inst. (2022), doi:10.1016/j.proci.2022.07.068.